Higher-Order Statistics of a Turbulent Jet in a Confined Crossflow

G. D. Catalano*
Louisiana State University, Baton Rouge, Louisiana 70803
J. A. Mathis†
Wichita State University, Wichita, Kansas 67208
and
K. S. Chang‡
Korean Advanced Energy Institute, Seoul, Korea

Higher-order statistics of the streamwise velocity and its time derivative have been measured in the plane of symmetry of a jet in a confined crossflow. The existence of universal similarity of the fine-scale structure of a developing turbulent velocity field and the validity of the original Kolmogorov local similarity theory and later formulations were investigated. Construction of normalized spectra for energy content, dissipation, and higher-order moments enabled an examination of the Reynolds number dependence of these functions for the Re_λ range from 16 to 800. Estimates of the Kolmogorov constant μ ranging from 0.27 to 0.43 were obtained with the arithmetic average equal to 0.38. The fractal dimension of the fine-scale structure was estimated from the functional relationship between the flatness of the velocity time derivative and Re_λ. For unfiltered data, the fractal dimension was estimated to be 2.45. However, with a $\pm 12\sigma$ bandwidth, the fractal dimension increased to 2.73.

I. Introduction

THE applicability and the limitations of the universal similarity theory first proposed by Kolmogorov[1] with subsequent clarifications by Kolmogorov,[2,3] Obukhov,[4] and Yaglom[5] continue to be the focus of many investigations. A larger data base of experimental results is required to establish the appropriate flow conditions for such theories.

The present work seeks to examine the suitability of flow models derived from the universal similarity theories in the case of a developing flow. The models examined include the Kolmogorov (LN) model,[3] the Novikov-Stewart (N-S) model,[6] and the Frisch, Sulem, and Nelkin (β) model.[7] The importance of the turbulent Reynolds number ($Re_\lambda = u\lambda/\nu$) is determined for various statistical properties of the flow. Such properties include the energy and dissipation spectra, the skewness, and the kurtosis. In addition, the applicability of fractal geometry to fine-scale structures in a developing flow is also examined.

II. Background

For relatively high Reynolds number flows, the energy containing large-scale turbulent eddies is unevenly distributed in space along with bursts of high-frequency fine-scale structures separated by periods of relative quiet. This observation led to refinements of Kolmogorov's first and second hypothesis by Kolmogorov[3] as well as by Obhukov[4] and Yaglom.[5] Kolmogorov's third hypothesis models as a lognormal random variable the locally averaged viscous dissipation of the turbulent kinetic energy. Mathematically

$$\sigma^2 = A + \mu \ln (l/r) \qquad \text{with} \qquad l \gg r \gg \eta \tag{1}$$

where σ^2 is the standard deviation of the logarithm of the viscous dissipation rate, l is the integral length scale of the flow, A is a constant depending on flow geometry, r is the characteristic length of the averaging volumes, η is the Kolmogorov length scale, and μ is a universal constant.

The existence of a universal equilibrium range and an inertia subrange are consequences of Kolmogorov's original theory.[1,2] The first hypotheses of similarity states that within an equilibrium range of wave numbers there exists a nondimensional and universal function Φ_1 such that for a locally isotopic field

$$\Phi_1(\eta k_1) = \frac{F_1(k_1)}{(\epsilon\nu^5)^{1/4}} \tag{2}$$

where

$$\overline{u_1^2} = \int_0^\infty F_1(k_1)\, dK_1 \tag{3}$$

where u_1 is the velocity fluctuation component in the mean flow direction x_1; ϵ is the viscous dissipation of the turbulent energy; ν is the kinematic viscosity; and $\eta = (\nu^3/\epsilon)^{1/4}$, the Kolmogorov length scale. For this to be valid, $Re_\lambda^{3/4} \gg 1$. The Reynolds number Re_λ used to characterize the turbulence is defined by

$$Re_\lambda = \overline{(u_1^2)}^{1/2}\lambda/\nu \tag{4}$$

where λ is the Taylor microscale. Kolmorogorov's second hypothesis is that for an even larger Reynolds number, $Re_\lambda^{3/8} \gg 1$, there exists a subrange of wave numbers within the equilibrium region where the effects of viscosity are negligible.[1,2] The one-dimensional spectrum function takes the form

$$F_1(k_1) = \alpha_1 \epsilon^{2/3} k_1^{-5/3} \tag{5}$$

With the assumption of a lognormal viscous dissipation according to Kolmogorov's third hypothesis[3]:

$$F_1(k_1) = \alpha_1 \epsilon^{2/3} k_1^{-5/3 - 1/9\mu} \tag{6}$$

Gurvich and Yaglom[8] provided a mathematical basis for the LN model assumptions. Gurvich and Yaglom[8] also concluded

Received Feb. 26, 1990; revision received Oct. 8, 1990; accepted for publication Oct. 8, 1990.

*Associate Professor, Department of Mechanical Engineering. Member AIAA.
†Assistant Professor, Department of Mechanical Engineering.
‡Researcher, Nuclear Energy Division.

that the probability density function of any non-negative quantity associated with the fine-scale structure of turbulence is approximately lognormal with a variance similar to l. Novikov and Stewart[6] proposed a model, the N-S model, for the spectrum of the dissipation spectrum Φ_ϵ, such that $\Phi_\epsilon \alpha k^{-1+\mu}$. This was also obtained by Gurvich and Yaglom[8] for $\mu < 1$.

Frisch et al.[7] introduced a model called the β model of fine-structure intermittency. For the β model

$$F_1(k_1) - k_1^{-5/3-1/3\mu} \tag{7}$$

Experimental tests of the Kolmogorov third hypothesis and attempts to evaluate the constant μ have been performed in both the laboratory and in high Reynolds number atmospheric boundary-layer flows by Pond and Stewart,[9] Gibson et al.,[10] Stewart et al.,[11] and Gibson et al.[12] Averaged dissipation rates have been studied by Van Atta and Chen[13] who measured streamline velocity derivatives for flow above the ocean. Yaglom[5] has provided a physical basis for Kolmogorov's third hypothesis. Mandelbrot[14] has shown this hypothesis to be probably untenable. A variant of the generating model leading to the lognormal has been proposed by Van Atta and Antonia,[15] who have examined the influence of fluctuations in the rate of local turbulent energy dissipation on higher-order structure functions for small separation distances and on moments of turbulent velocity derivatives using the hypothesis of Kolmogorov[3] and Obukhov.[4] The derivatives of the dissipation rates of turbulent velocity and temperature fields were observed by Gibson and Masiello.[16] Departures from lognormality of the averaged squared derivatives were present at lower Reynolds numbers. This proved to be contrary to the proposal of Gurvich and Yaglom.[8]

Experiments have yielded a wide range of values of μ. Gibson and Masiello[16] found the most probable value is within a range 0.17–0.80. Yaglom[5] estimated a value of 0.4, Antonia et al.[17] suggested a value of $\mu = 0.2$ from their investigations of circular and plane jets along the axes of symmetry. Difficulties in comparing experimental results appear to be attributable to the questionable universality of μ.

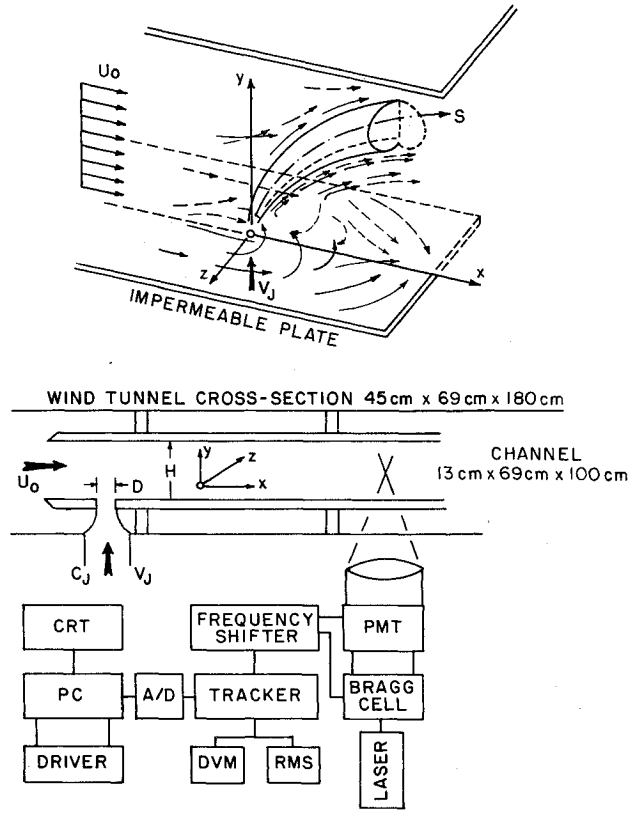

Fig. 1 Schematics of the flowfields and the laser Doppler velocimeter.

The kurtosis or flatness of $\partial u_1/\partial x_1$ is defined as

$$K = \overline{\left(\frac{\partial u_1}{\partial x_1}\right)^4} \Big/ \left[\overline{\left(\frac{\partial u_1}{\partial x_1}\right)^2}\right]^2 \tag{8}$$

Assuming local isotropy and the applicability of Taylor's hypothesis,

$$U_1 \frac{\partial u_1}{\partial t} = \frac{\partial u_1}{\partial x_1} \tag{9}$$

or

$$K = \overline{\left(\frac{\partial u_1}{\partial t}\right)^4} \Big/ \left[\overline{\left(\frac{\partial u_1}{\partial t}\right)^2}\right]^2 \tag{10}$$

Sreenivasan and Meneveau[18] have shown that

$$K\alpha\left(\frac{1}{\eta}\right)^{3-D} \tag{11}$$

or

$$K\alpha Re_\lambda^{3/2(3-D)} \tag{12}$$

where D is the fractal dimension of the dissipative field in a turbulent flow.

III. Experimental Design and Accuracy of Data

An axisymmetric turbulent jet exhausting into a confined crossflow has been chosen for this investigation and is shown in Fig. 1. The flowfield that results is a basic configuration that finds application in V/STOL aerodynamics, the design of gas turbine combustors, the internal cooling of turbine blades, and hazardous waste management. The noteworthy features of this configuration are the bending of the jet, the upward and sideways movement of the mainstream, the reverse flow downstream of the jet, the presence of two vortices in the kidney-shaped cross section of the jet, and the impingement region.

The present experiments are performed in a subsonic wind tunnel with the dimensions of the test section equal to 68 cm wide, 45 cm high, and 180 cm long. The nearly uniform flow in the test section is attained by routing the airflow through a 12:1 contraction section and flow straightening honeycomb tubes. The freestream turbulent intensity is less than 0.8% in the range of tunnel velocities U_0 (9.5–50.0 m/s). Optical access for the laser Doppler anemometer (LDA) measurements is provided through a removable plexiglass wall in the test section.

The jet stream is supplied from the laboratory's compressed air system and adjusted by a high-precision pressure regulator. To minimize the affect of the tunnel wall boundary layer, the jet exit is mounted flush onto a flat plate placed 12 cm above the bottom wall of the tunnel, and the jet is aligned with the test section centerline. The maximum obtainable jet velocity U_j is approximately 50.0 m/s and the corresponding Reynolds number based on the 1.27-cm jet diameter is 3.9×10^4. The dimensions of the confining channel are 12.7 cm in the vertical direction and 68.6 cm in the lateral direction.

The velocity ratio values, $\lambda_j = U_j/U_0$, are achieved by adjustment of the compressed air line pressure regulator on the jet flow system while keeping the tunnel flow fixed at 9.5 m/s. The assumption of symmetry of the entire flowfield about the plane $z = 0$ was also validated. In the work presented here, all experimental data was obtained in the plane of symmetry.

The details of the LDA set up are as follows: beam intersection angle, $\theta = 7.25$ deg; fringe spacing, $d_f = 5$ μm; probe volume diameter, $d_{pv} = 0.25$ mm; probe volume length, $l_{pv} = 3.6$ mm; He-Ne laser rated at 15 mW, $\lambda_{laser} = 632.8$ nm.

Table 1 Sources of error

Calibration	Calibration error: Bias limit, ± V	Calibration error: Precision index, ± V
Excitation voltage	$B_{11} = 0.0010$	$P_{11} = 0.0010$
Tracker	$B_{21} = 0.0500$	$P_{21} = 0.0200$
A/D converter	$B_{31} = 0.0020$	$P_{31} = 0.0010$

$$B_1 = [B_{11}^2 + B_{21}^2 + B_{31}^2]^{1/2} = 0.0501 \text{ V}$$

$$P_1 = [P_{11}^2 + P_{21}^2 + P_{31}^2]^{1/2} = 0.0201 \text{ V}$$

Error source	Data acquisition error: Bias limit, ± V	Data acquisition error: Precision index, ± V
Frequency shifter	$B_{12} = 0.0100$	$P_{12} = 0.0050$
Excitation voltage	$B_{22} = 0.0050$	$P_{22} = 0.0050$
Tracker	$B_{32} = 0.0100$	$P_{32} = 0.0050$
A/D converter	$B_{42} = 0.0020$	$P_{42} = 0.0020$
Atmospheric conditions	$B_{52} = 0.0000$	$P_{52} = 0.0050$
Positioning error	$B_{62} = 0.0000$	$P_{62} = 0.0100$
Velocity bias error	$B_{72} = 0.0050$	$P_{72} = 0.0000$

$$B_2 = [B_{12}^2 + B_{22}^2 + \cdots + B_{72}^2]^{1/2} = 0.0159 \text{ V}$$

$$P_2 = [P_{12}^2 + P_{22}^2 + \cdots + P_{72}^2]^{1/2} = 0.0143 \text{ V}$$

Error source	Data reduction error: Bias limit, ± V	Data reduction error: Precision index, ± V
Computer resolution	$B_{13} = 0.0020$	$P_{13} = 0.0000$

$$B_3 = 0.0020, \; P_3 = 0.0000$$

The optics are manufactured by DANTEC (55X Modular Optics). The jet stream and the freestream are seeded with olive oil particles using an aerosol generator. The mean oil droplet diameter is estimated to be 1.0 μm. This particle diameter range is appropriate to follow air flows where turbulence frequencies exceed 1 kHz.

The data acquisition system is composed of a TSI Model 1090 tracker processor, a DANTEC counter used solely for amplification and filtration, and a Zenith Z248 personal computer. The analog output of the tracker is sent to the computer that is equipped with an OMEGA WB-800 data acquisition A/D board. The data acquisition rate is set at 38 kHz. The number of data samples obtained and stored at each flow location is 28,400. The data records, stored on micro floppy diskettes, are transferred to the main frame, IBM 3090 computer for statistical analysis.

The difficulty in obtaining reliable measurements of small-scale turbulence has been discussed by previous investigators. Tennekes and Wyngaard[19] discussed signal-to-noise and integration time limitations that make measurements of moments greater than the fourth difficult for large Reynolds number flows. Frenkiel and Klebanoff[20] discussed effects such as averaging intervals and convergent tails of the probability density functions. Champagne[21] discussed the credibility of the results of previous investigators and devised three important criteria for the elimination of results. If the length of the sensors is much greater than the Kolmogorov microscale, or the low-pass filter setting is equal to or less than the Kolmogorov frequency, then the data are suspect. Additionally, inadequate averaging time results in excessive scatter. Antonia et al.[22] considered two further points that were the closure of the tails of the probability density functions and the effect of Taylor's hypothesis.

Size of Measuring Volume

The spatial resolution of the sensor is clearly important to the study of the fine structure. The ratio of length l_{pv} (= 3.6 mm) to diameter d_{pv} (= 0.25 mm) is 14.4. The Kolmogorov scales measured ranged from $\eta_{\min}$ (= 0.17 mm) to $\eta_{\max}$ (= 1.01 mm). The ideal sensor would require $l_{pv}/\eta \leq 1$ and $d_{pv}/\eta \leq 1$. In the present investigation $l_{pv}/\eta = 21$ and $d_{pv}/\eta = 1.5$. The correctional approach of Schedvin et al.[23] was not used. This is in agreement with the work by Antonia et al.[22]

Frequency Response

The cut-off frequency setting for the DANTEC filters was determined at each measurement location. It was initially set arbitarily equal to a frequency typically twice the upper limit of the spectral content of u_1. The spectral density Φ obtained using a real-time spectrum analyzer was first displayed on the built-in oscilloscope of the analyzer to determine f_c visually as described by Antonia et al.[22] For the present experimental conditions, it was found that for all flowfield locations, the value of f_c was slightly greater than 1.5 f_η.

Integration Time

To reach a stable value for higher orders of moment requires a longer integration time.[22] Tennekes and Lumley[24] estimated this time by the relation

$$w^2 = 2\left(\frac{\overline{\dot{u}_1^{2n}}}{(\overline{\dot{u}_1^n})^2} - 1\right)\frac{I_n}{T} \tag{13}$$

where w^2 is the mean square relative error of $\overline{\dot{u}_1^n}$, T is the total record derivation, and I_n is the integral time scale of $z_n(\equiv \dot{u}_1^n - \overline{\dot{u}_1^n})$ defined as

$$I_n = \frac{1}{\overline{z_n^2}}\int_0^\infty \overline{z_n(t)z_n(t+\tau)}\, d\tau \tag{14}$$

Sreenivasan et al.[25] have approximated the reduction in I_n as n increases as

$$\frac{I_n}{I_1} = 0.82 - 0.07n \tag{15}$$

In the present investigation, T(= 0.738 s) was fixed, selecting an upperbound on the Kolmogorov microscale η(= 1×10^{-5} m) and TU_1/L_0 (= 1×10^3) (where L_0 is a characteristic transverse distance) and assuming a longitudinal mean velocity U_1 (= 10 m/s), then the mean-square relative error for the flatness of the velocity derivative was less than 2%. The mean-square error of the skewness was similarly estimated to be less than 1%.

Convergence of Probability Density Function

The average value of $\dot{u}_1^n$ can be written as

$$\overline{\dot{u}_1^n} = \dot{u}_1^n \, p(\dot{u}_1)\, d\dot{u} \tag{16}$$

where the probability density function is

$$\int p(\dot{u}_1)\, d\dot{u}_1 = 1 \tag{17}$$

Careful attention must be paid to the close of the probability density function tails. Values of $\overline{\dot{u}^n}$ were computed directly from the digital record and also using the probability density function. The visual curve fits yielded results within 20% of the value obtained from the digital record. Closure of the tails of $p(\dot{u}_1)$ was reasonable even at $n = 6$, thus indicating that the dynamic range of the signal-processing equipment was satisfactory.

Consideration of Fluctuating Convection Velocity Effects

Champagne[21] applied corrections to several statistics of $\dot{u}$ due to the effect of a fluctuating convection velocity on Taylor's hypothesis. An overestimate of the mean dissipation for flow locations with high turbulence results because

$$\overline{\dot{u}_1^2} = \overline{U^2\left(\frac{\partial u_1}{\partial x_1}\right)^2}\left(1 + \frac{\overline{u_1^2}}{U^2} + \frac{2(\overline{u_2^2} + \overline{u_3^2})}{U^2}\right) \tag{18}$$

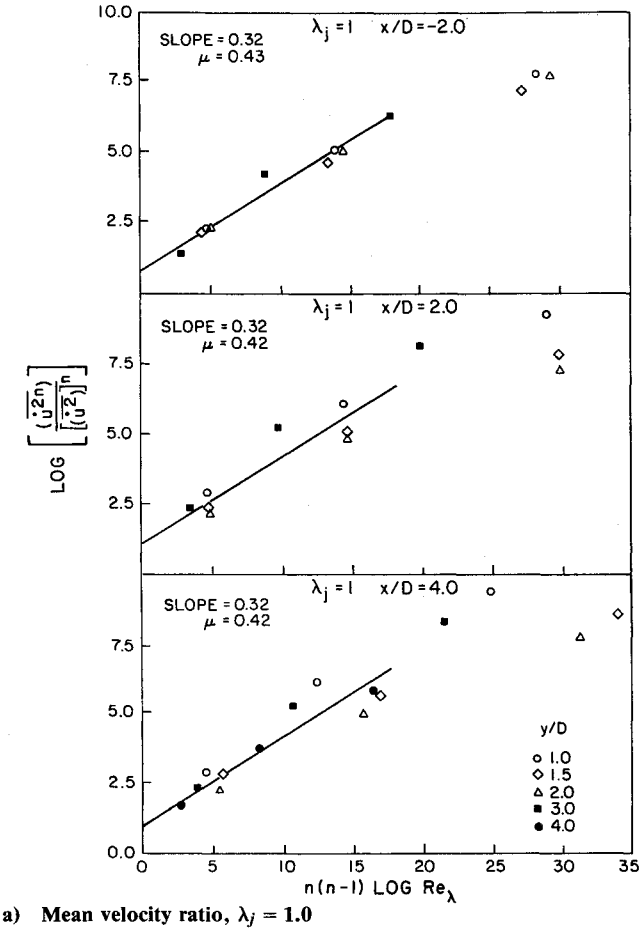

a) Mean velocity ratio, $\lambda_j = 1.0$

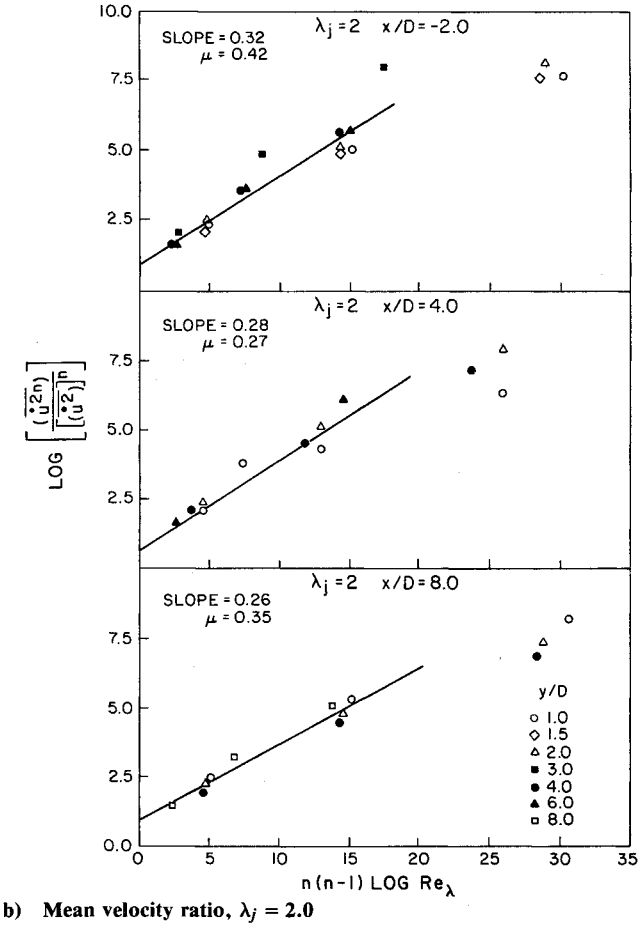

b) Mean velocity ratio, $\lambda_j = 2.0$

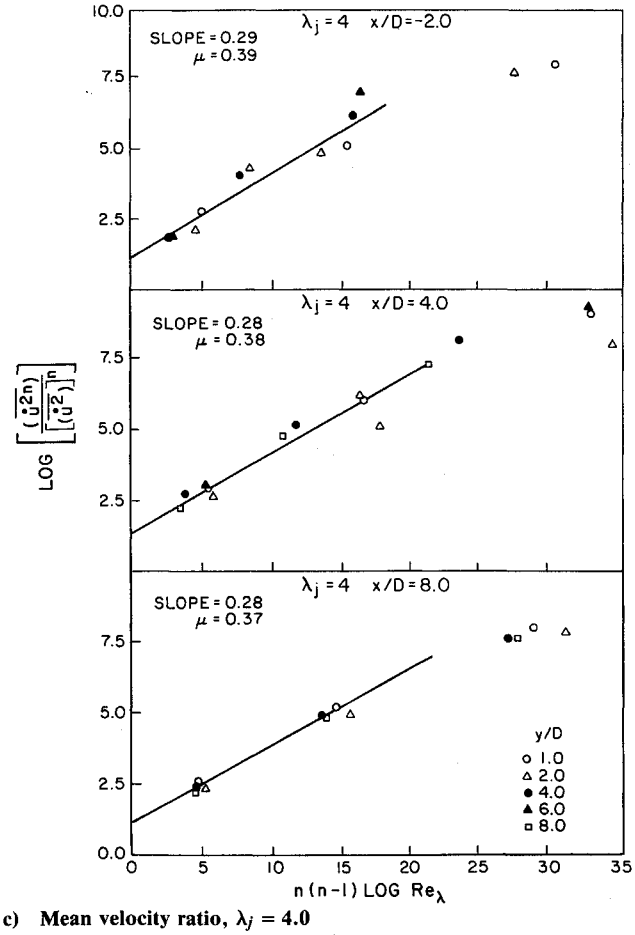

c) Mean velocity ratio, $\lambda_j = 4.0$

Fig. 2 Reynolds number dependency of $\overline{(\dot{u}^{2n})}/\overline{(\dot{u}^2)}^n$ vs $n(n-1)$ log Re_λ; for various flow locations.

The use of this formula in the present experimental investigation indicates that $\overline{(\partial u_1/\partial x_1)^2}$ is underestimated by about 2%. Antonia et al.[17] have discussed the assumptions underlying Eq. (18) and concluded that since little is known about $\partial u_1/\partial x_1$, statistics of $\partial u_1/\partial x_1$ formed by decoupling $\dot{u}_1$ by $U_1 + u_1$ may be preferred. Antonia et al.[17] found that

$$\overline{\dot{u}_1^2} = U^2\overline{\left(\frac{\partial u_1}{\partial x_1}\right)^2}\left(1 + 3\frac{\overline{u_1^2}}{U_1^2} + 5\frac{\overline{u_1^4}}{U_1^4}\right)^{-1} \tag{19}$$

Application of this formula to the present measurement indicates that $\overline{(\partial u_1/\partial x_1)^2}$ is underestimated by about 2%. Antonia et al.[17] noted that further work was required before a choice could be made between Eqs. (18) and (19). Before such an investigation, no corrections have been made in the present work to either second- or higher-order increments as suggested by Antonia et al.[17]

Other Comments on Errors

The measurements and results presented in this study are meaningless without an estimate of the errors involved. The ANSI/ASME[26] procedure for calculating and reporting measurement uncertainty is followed here.

Errors are divided into three categories: calibration errors, data acquisition errors, and data reduction errors. For each source of error, there is a bias and a precision component. A bias error is a constant or systematic error present for the duration of the test. Precision error is random error; the measure of precision error is the statistic sample standard deviation. Error values are estimated from manufacturer's literature, by comparison of error estimates of similar equipment, by experimentation, and by the authors' judgment. Estimates of the various components of error are indicated in Table 1.

Table 2 Statistical documentation for various velocity ratios and flow locations

Velocity ratio, $\lambda_j = 4.0$									
x/D	y/D	l, m	$\lambda \times 10^2$, m	v_η, m/s	$\eta \times 10^4$, m	ϵ, m^2/s^3	Re_λ	K	S
+8	+1	0.0626	0.603	0.465	0.344	2,929	260	335	−5.50
	+2	0.0741	0.794	0.510	0.314	4,218	407	228	−2.02
	+4	0.053	0.479	0.453	0.353	2,637	181	245	−0.08
	+6	0.0323	0.446	0.472	0.339	3,100	178	285	−1.03
	+8	0.0544	0.550	0.353	0.454	967	209	134	−2.10
+4	+1	0.157	0.905	0.761	0.210	20,918	567	624	−2.06
	+2	0.128	0.711	0.740	0.216	18,727	512	211	1.05
	+4	0.0944	0.396	0.746	0.214	19,351	114	1367	0.070
	+6	0.438	1.25	0.495	0.323	3,750	582	1002	0.065
	+8	0.0456	0.431	0.243	0.658	218	63	199	0.085
−2	+1	0.0659	0.748	0.473	0.338	3,125	358	340	2.10
	+2	0.0913	0.711	0.344	0.465	873	197	199	1.06
	+4	0.177	0.257	0.184	0.871	713	22.1	66.4	0.95
	+6	0.0699	0.286	0.186	0.860	75	24.4	80.1	0.92
Velocity ratio, $\lambda_j = 2.0$									
x/D	y/D	l, m	$\lambda \times 10^2$, m	v_η, m/s	$\eta \times 10^4$, m	ϵ, m^2/s^3	Re_λ	K	S
+8	+1	0.129	0.694	0.569	0.281	6,550	384	352	−2.05
	+2	0.0421	0.543	0.553	0.289	5,860	274	204	2.16
	+4	0.0438	0.535	0.411	0.389	1,790	243	105	−3.78
	+8	0.0146	0.199	0.166	0.965	47.15	15	39.6	−0.088
+4	+1	0.0178	0.320	0.595	0.269	7,853	158	119	−4.05
	+2	0.0283	0.366	0.587	0.272	7,440	165	329	−5.47
	+4	0.0302	0.418	0.288	0.555	432	99.8	124	−4.56
	+6	0.0126	0.210	0.172	0.930	54.7	17.2	52.3	0.075
	+8	0.0132	0.207	0.169	0.948	50.77	16.7	33.7	0.011
−2	+1	0.130	0.735	0.518	0.309	4,503	345	248	0.010
	+2	0.0887	0.742	0.379	0.423	1,283	262	322	−0.026
	+4	0.0188	0.239	0.158	1.01	39.2	17.2	37.9	−0.028
	+6	0.0243	0.228	0.175	0.916	58.3	18.9	41.9	−0.005
Velocity ratio, $\lambda_j = 1.0$									
x/D	y/D	l, m	$\lambda \times 10^2$, m	v_η, m/s	$\eta \times 10^4$, m	ϵ, m^2/s^3	Re_λ	K	S
+4	+1	0.125	0.331	0.996	0.161	61,600	124	824	−4.5
	+1.5	0.184	1.04	0.667	0.240	12,300	714	503	2.3
	+2	0.0838	0.827	0.442	0.362	2,390	425	226	−1.8
	+3	0.0241	0.376	0.246	0.651	228	65.2	189	−1.95
	+4	0.0214	0.278	0.170	0.943	51.8	24.3	43.6	−0.05
+2	+1	0.179	0.552	0.948	0.169	50,500	277	756	−2.05
	+1.5	0.303	0.681	0.417	0.383	1,900	317	269	−1.55
	+2	0.0722	0.647	0.437	0.367	2,276	326	185	−1.95
	+3	0.045	0.369	0.216	0.740	137	48.2	236	−1.95
−2	+1	0.0578	0.588	0.421	0.380	1,970	214	254	−0.75
	+1.5	0.0309	0.488	0.392	0.410	1,480	177	157	−1.12
	+2	0.0594	0.667	0.391	0.408	1,460	258	199	0.08
	+3	0.0359	0.321	0.189	0.846	79.9	32.3	74.5	0.65

The total bias and precision errors are calculated by the root-sum-square method:

$$B = (B_1^2 + B_2^2 + B_3^2)^{1/2} = 0.0526 \text{ volts} \quad (20)$$

$$P = (P_1^2 + P_2^2 + P_3^2)^{1/2} = 0.0247 \text{ volts} \quad (21)$$

The final uncertainty ψ is obtained by combining bias and precision errors. The 95% confidence level interval[26] is given by

$$\psi_{95} = [B^2 + (tP)^2]^{1/2} \quad (22)$$

Here, t is the student-t value and is a function of the number of degrees of freedom used in calculating P. For precision indices associated with electronic equipment,[26] a large number of degrees of freedom justifies choosing t as 2.0 or

$$\psi_{95} = \{(0.0526)^2 + [2(0.0247)]^2\}^{1/2} \quad (23)$$

$$= 0.0722 \text{ volts} = 0.36 \text{ m/s} \quad (24)$$

A velocity measurement may therefore be expected, with a 95% confidence level, to lie within ± 0.36 m/s of the experimentally obtained value. For the range of velocity values obtained in this study, this corresponds to between 13.6 and 3.40% error, maximum.

IV. Results

An exhaustive documentation of the turbulent jet in a confined crossflow has already been performed and has been documented in the technical literature (Catalano et al.[27]). Our purpose here is to concentrate on the fine-scale turbulent structure. The first task at hand is a determination of the proposed universal constant μ.

Estimates of μ

The dependence of the Reynolds number Re_λ and order n of higher even-order moments

$$\overline{\left(\frac{\partial u_1}{\partial t}\right)^{2n}} \Big/ \left[\overline{\left(\frac{\partial u_1}{\partial t}\right)^2}\right]^n$$

for $n = 2,3,4$ is plotted in Fig. 2. Frenkiel and Klebanoff,[20] using the properties of the lognormal distribution, showed that

$$\overline{\left(\frac{\partial u_1}{\partial t}\right)^{2n}} \Big/ \overline{\left(\frac{\partial u_1^2}{\partial t}\right)^{n}} \sim \left(\frac{L}{\eta}\right)^{\frac{1}{2}\mu n(n-1)} \sim Re_\lambda^{\frac{1}{4}\mu n(n-1)} \qquad (25)$$

under the isotropic assumption that $L/\eta \sim Re_\lambda^{3/2}$. The local slope of the experimental distribution of Fig. 2 is proportional to μ and thus the plots shown in Fig. 2 can be thought of as a possible method for determining μ. Nine sets of experimental data are presented corresponding to different velocity ratios ($\lambda_j = 1,2,4$) and flow locations ($x/D = -2,4,8$). A straight line has been fitted up to a value of $n(n-1)$ log Re_λ of approximately 20. The arithmetic average value of m is estimated to be 0.38 obtained from a power curve fit with a coefficient of correlation equal to 0.95. It has been suggested by Frenkiel and Klebanoff[20] and Antonia et al.[17] that the decrease of μ with n is universal for a given value of f_c in the sense that it does not depend on the particular flow. The present data provide further support for this suggestion. A comparison with the previous results also indicates a slightly higher value of the even-order moments.

The implications of these results are significant. First, the magnitude of μ for this particular flow is quite close to the value originally predicted by Yaglom[5] ($\mu = 0.4$). This value is considerably higher than the value proposed by Antonia et al.[17] ($\mu = 0.2$) and less than the estimate of Gibson and Masiello[16] ($\mu = 0.5$). Second, the particular flowfield investigated in this work must be considered developing rather than fully developed. Hence, it would seem arguable that the fully developed restriction may be relaxed and the universal equilibrium theories may apply to the near-field problem in turbulence as well.

Skewness and Flatness Factors of the Velocity Derivatives

Flatness K and skewness S factors of $\partial u_1/\partial t$ are presented in Table 2. Several general observations may be made. First, although the largest flatness values of skewness are found at larger flatness values, distributions with large flatness values appear to be equally likely to have large or small values of skewness. The flatness values range from 30 to 1000. These large flatness values indicate a higher than normal probability of values far from the mean, and the non-Gaussian nature of the derivatives is evident. Predictions of the relationship between flatness and skewness predicted by the lognormal model ($S \alpha K^{3/8}$) or by the β model ($K \alpha S^2$) are not indicated by this data. The flatness is seen to increase monotonically with the turbulent Reynolds number (note that v_k is the Kolmogorov velocity scale).

One-Dimensional Energy Spectra

The one-dimensional energy spectra is $F_1(k_1)$ whose integral over all wave numbers is $\overline{u_1^2}$. Taylor's approximation in the form $k_1 = 2\pi f/U_1$ was used to transform the frequency f to the wave number k_1, the x_1 component. The spectra are presented here in Kolmogorov-normalized form, i.e., divided by $(\epsilon\nu^5)^{1/4}$ as indicated by Eq. (2), in Fig. 3a. The value of the dissipation rate ϵ was estimated from the second moment of the dimensional spectra (Fig. 3b) using the assumption of dissipative local isotropy, or

$$\epsilon = 15\nu \int_0^\infty k_1^2 F_1(k_1)\, dk \qquad (26)$$

Variation of the functions $(\eta k)^2\Phi(\eta k)$, $(\eta k)^{5/3}\Phi(\eta k)$, and $(\eta k)^4\Phi(\eta k)$ with Re_λ is examined. The maximum values from each function are plotted against Re_λ in Figs. 4a–4c. Variation

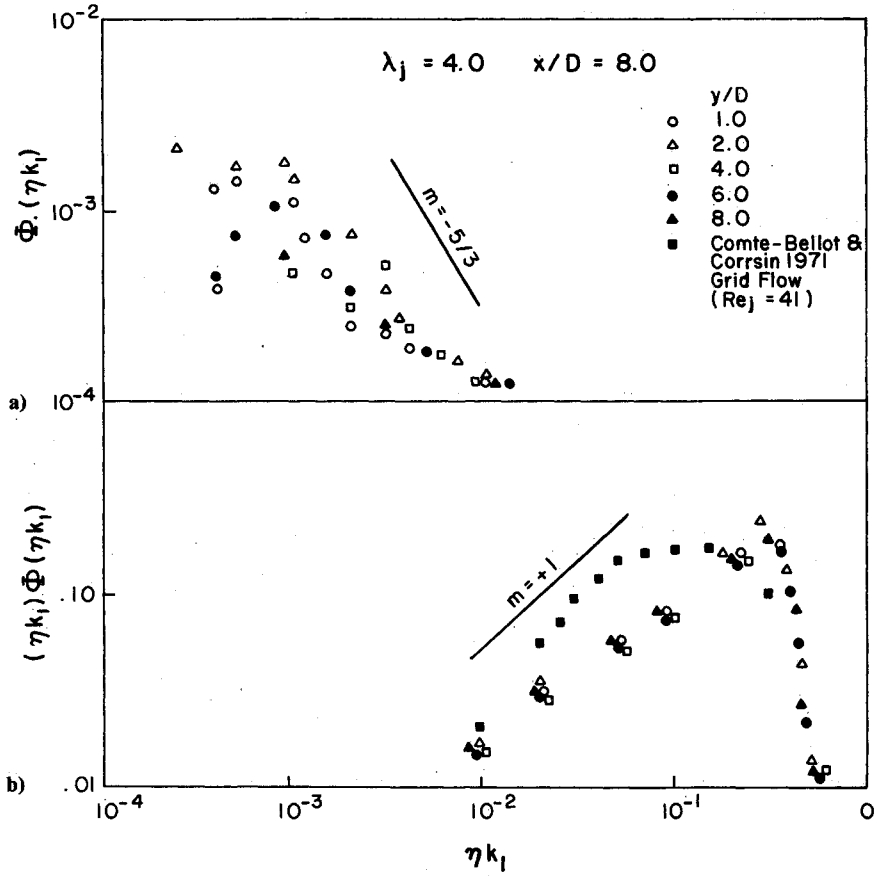

Fig. 3 Example of typical nondimensionalized spectra for $\lambda_j = 4.0$ and $x/D = 8.0$ at various locations between the plates. a) Energy spectra: $y/D = 1.0$, $Re_\lambda = 260$; $y/D = 2.0$, $Re_\lambda = 407$; $y/D = 4.0$, $Re_\lambda = 189$; $y/D = 6.0$, $Re_\lambda = 178$; $y/D = 8.0$, $Re_\lambda = 209$. b) Dissipation spectra, comparison to grid flow data from Champagne[21]: $y/D = 1.0$, $Re_\lambda = 260$; $y/D = 2.0$, $Re_\lambda = 407$; $y/D = 4.0$, $Re_\lambda = 189$; $y/D = 6.0$, $Re_\lambda = 178$; $y/D = 8.0$, $Re_\lambda = 209$.

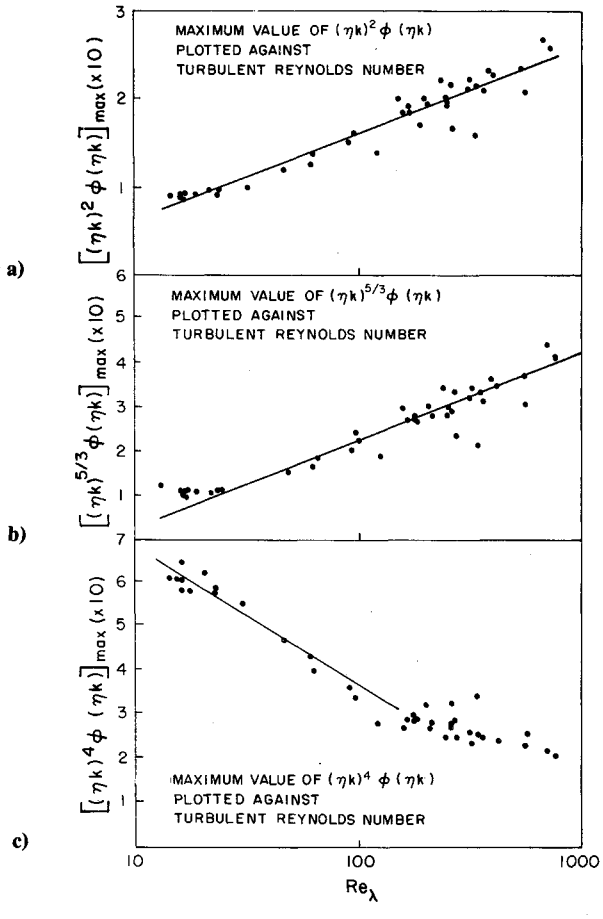

Fig. 4 Maximum values of $(\eta k)^2 F(\eta k)$, $(\eta k)^{5/3} \Phi(\eta k)$, and $(\eta k)^4 \Phi(\eta k)$ plotted vs turbulent Reynolds number at various downstream locations.

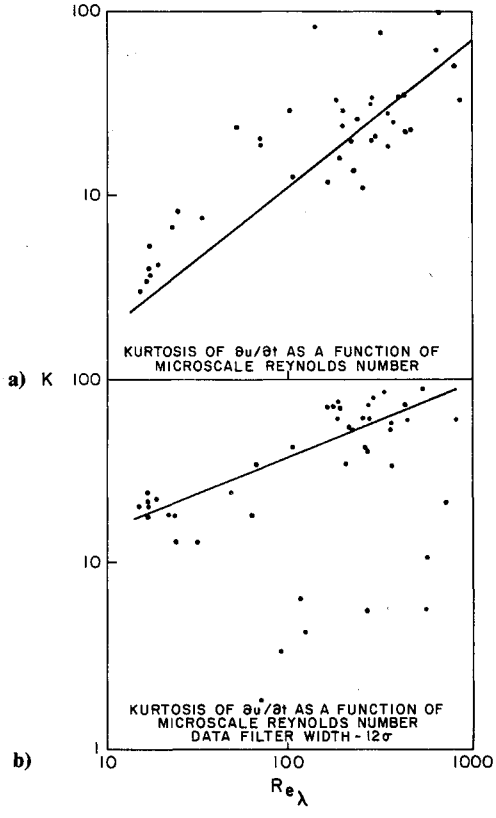

Fig. 5 Kurtosis of the velocity derivative as a function of the turbulent or microscale Reynolds number for two cases: a) without numerical filter, b) with numerical filter, $\pm 12\sigma$.

of these maximum values was found to vary with the logarithm of Re_λ. For $(\eta k)^2\Phi(\eta k)$, the relationship

$$M_1 = 0.0413 \log Re_\lambda - 0.0326, \qquad 10 < Re_\lambda < 1000 \tag{27}$$

was obtained, where M_1 denotes the maximum value of $(\eta k)^2 \Phi(\eta k)$. The coefficient of correlation for the curve is 0.96. For the function $(\eta k)^{5/3}\Phi(\eta k)$, a similar relationship was found to be (M_2 is the maximum)

$$M_2 = 0.0856 \log Re_\lambda - 0.171, \qquad 10 < Re_\lambda < 1000 \tag{28}$$

with a coefficient of correlation of 0.95. Finally, for $(\eta k)^4 \Phi(\eta k)$, the variation obtained was (M_3 is the maximum)

$$M_3 = 0.1009 - 0.0140 \log Re_\lambda, \qquad 10 < Re_\lambda < 150 \tag{29}$$

with coefficient of correlation 0.98. For values of Re_λ greater than 150, the peak values displayed a decreased dependence on Re_λ.

Some comparisons with earlier studies can be made. Dissipation spectra from Frenkiel and Klebanoff[20] have been presented. For $Re_\lambda = 60.8$, they found the maximum value of $(\eta k)^2\Phi(\eta k)$ to be 0.22. For $Re_\lambda = 45.2$, the corresponding maximum was 0.19. The correlation determined in this study, Eq. (27), would predict $M = 0.14$ for $Re_\lambda = 60.8$ and $M = 0.12$ for $Re_\lambda = 45.2$. Champagne[21] compiled and graphed $(\eta k)^2 \Phi(\eta k)$ from four research sources of varying Reynolds number: 1) a cylinder wake flow, $Re_\lambda = 138$, 2) a grid flow, $Re_\lambda = 41$, 3) a grid flow, $Re_\lambda = 65$, and 4) a homogeneous shear flow, $Re_\lambda = 130$. These curves were found to be very nearly the same, leading Champagne to conclude that the fine-scale structure of the different flowfields is similar at least for the Re_λ range presented here, viz., 40–138. The results obtained here indicate that for this developing flowfield Reynolds number independence is not found either for $40 < Re_\lambda < 138$ or for the entire range investigated, $16.6 < Re_\lambda < 782$.

Fractal Dimension of the Dissipation Structure

The fractal dimension D of the dissipation structure was determined from calculations of the turbulent Reynolds number and the flatness of the velocity derivatives at each measuring location. Figure 5 shows a plot of the results. The slope of the line is 0.823, calculated by least-squares nonlinear regression and having a correlation coefficient of 0.77. The relationship

$$K \propto Re_\lambda^{3/2(3-D)} \tag{30}$$

becomes

$$K = 2.72 Re_\lambda^{0.823} \tag{31}$$

giving a fractal dimension $D = 2.45$.

Sreenivasan and Meneveau[18] reported a fractal dimension value of 2.73–2.78, based on a collection of research data. A comparison made of the flatness values in the present work and the other research indicated a possible explanation for the discrepancy. The flatness values found in this study are up to an order of magnitude larger than flatness factors reported elsewhere for flows of comparable Re_λ. Some of the increases may be attributable to the developing nature of the flow in this study, where large variations in velocity occur due to the complex superposition of different flow patterns. However, the developing (vs fully developed) nature of the flow cannot be considered completely responsible for the difference in flatness values. The main reason for the discrepancy, however, may be different measuring techniques used. The velocity derivative values in this research were calculated from digitized velocity data. It is possible that the digital velocity derivative calculations produced high and low values not discriminated by the analog instruments used in earlier studies.

To test what effect such a loss of high and low end data could have on the estimation of D, a "filter" was applied to our data. The width of the filter was set at 12 times the standard deviation of the sample and centered at its mean. New flatness factors were calculated for the filtered data and found to be substantially lower.

When the filtered data was plotted against Re_λ, as shown in Fig. 5, the slope of the resultant line led to a fractal dimension of $D = 2.73$, exactly in the range estimated by Sreenivasan and Meneveau.[18]

Sreenivasan and Meneveau[18] also reported fractal dimensions of the turbulent/nonturbulent surface in several types of turbulent shear flows (boundary layer, axisymmetric jet, plane wake, and mixing layer). They found an interface dimension of 2.3–2.4 that apparently was independent of the type of flow. It is interesting that the turbulent interface fractal dimension is close to the 2.45 fractal dimension of the dissipation structures.

V. Conclusions

The turbulent flowfield obtained by injecting a jet into a confined crossflow provided a convenient case where data could be collected to examine the fine-scale structure of turbulence in a developing flow over a large range of turbulent Reynolds numbers. Calculations indicated the range of turbulent Reynolds numbers to be 16.6–782, and the widely different values of integral length scale varying from 0.013 to 0.438 m confirmed the developing nature of the flow.

By directing the output of the signal-processing equipment to an analog/digital converter operating in a direct memory access mode with the laboratory computer, a data collection frequency of sufficient speed to capture the fine-scale fluctuations was attained. The digitized velocity values were then subjected to calculation procedures designed to extract statistical estimates of certain physically relevant quantities.

Construction of normalized spectra for energy content, dissipation, and higher-order moments enabled an examination of the Reynolds number dependence of these functions; the dependence was definite and well defined. Comparisons with other research data, however, indicated that this Reynolds number dependence has not been detected in some investigations of fully developed flows at comparable Reynolds numbers.

The value of the constant μ from Kolmogorov's lognormal hypothesis was calculated to average 0.38 over the range of turbulent Reynolds numbers sampled. Its Reynolds number dependence indicates the inappropriateness of the lognormal distribution to this flow as a whole.

The fractal dimension of the dissipative structures was estimated to be 2.45. An attempt to reconcile the discrepancy between this value and another reported estimate led to the tentative conclusion that the fractal dimension of this developing flow and the fractal dimension estimated for other developed flows encompassing a wide range of Reynolds numbers may be quite close.

References

[1]Kolmogorov, A. N., "Local Structure on Turbulence in Incompressible Fluid," *C. R. Acad. Sci. U.R.S.S.*, Vol. 30, 1941a, p. 299.

[2]Kolmogorov, A. N., "On Logarithmically-Normal Law of Distribution," *C. R. Acad. Sci., U.R.S.S.*, Vol. 31, 1941b, p. 599.

[3]Kolmogorov, A. N., "A Refinement of Previous Hypothesis Concerning the Local Structure of Turbulence in a Viscious Incompressible Fluid at High Reynolds Number," *Journal of Fluid Mechanics*, Vol. 13, Pt. 1, May 1962, pp. 82–85.

[4]Obukhov, A. M., "Some Specific Features of Atmospheric Turbulence," *Journal of Fluid Mechanics*, Vol. 13, Pt. 1, May 1962, pp. 77–91.

[5]Yaglom, A. M., *Sov. Phys. Dokl.*, Vol. 11, 1966, p. 26.

[6]Novikov, E. A., and Stewart, R. W., *Iz. Akad. Nauk. Ser. Geophys 3*, 1964, p. 408.

[7]Frisch, V., Sulem, P. L., and Nelkin, M., "A Simple Dynamical Model of Intermittent Fully Developed Turbulence," *Journal of Fluid Mechanics*, Vol. 87, Pt. 4, Aug. 1978, pp. 719–736.

[8]Gurvich, A. S., and Yaglom, A. M., *Physics of Fluids*, Suppl. 10, 1967, p. 559.

[9]Pond, S., and Stewart, R. W., *Izv. Atmos. Ocean. Phys.*, Vol. 1, 1965, p. 530.

[10]Gibson, C. H., Stegen, G. R., and Williams, R. B., "Statistics of Fine Structure of Turbulent Velocity and Temperature Fields at High Reynolds Numbers," *Journal of Fluid Mechanics*, Vol. 41, Pt. 1, March 1970, pp. 153–167.

[11]Stewart, R. W., Wilson, J. R., and Burling, R. W., "Some Statistical Properties of Small Scale Turbulence in an Atmospheric Boundary Layer," *Journal of Fluid Mechanics*, Vol. 41, Pt. 1, March 1970, pp. 141–159.

[12]Gibson, C. H., Stegen, G. R., and McConnell, S., "Measurements of the Universal Constant in Kolmogorov's Third Hypothesis for High Reynolds Number Turbulence," *Physics of Fluids*, Vol. 13, No. 10, 1970, pp. 2448–2451.

[13]Van Atta, C. W., and Chen, W. Y., "Structure Functions of Turbulence in Atmospheric Boundary Layer over the Ocean," *Journal of Fluid Mechanics*, Vol. 44, Pt. 1, Oct. 1970, pp. 145–159.

[14]Mandelbrot, B. B., "Intermittent Turbulence in Self Similar Cascades: Divergence of High Moments and Dimensions of Carrier," *Journal of Fluid Mechanics*, Vol. 62, Pt. 2, Jan. 1974, pp. 331–358.

[15]Van Atta, C. W., and Antonia, R. A., "Reynolds Number Dependence of Skewness and Flatness Factors of Turbulent Velocity Derivatives," *Physics of Fluids*, Vol. 23, No. 2, 1980, pp. 252–257.

[16]Gibson, C. H., and Masiello, P. J., *Statistical Models and Turbulence*, edited by M. Rosenblatt and C. W. Van Atta, *Lecture Notes in Physics*, Vol. 12, Springer Verlag, 1972, p. 427.

[17]Antonia, R. A., Phan-Thien, N., and Chambers, A. J., "Taylor's Hypothesis and the Probability Density Functions of Temporial Velocity and Temperature Derivatives in a Turbulent Flow," *Journal of Fluid Mechanics*, Vol. 100, Pt. 1, Sept. 1980, pp. 193–208.

[18]Sreenivasan, K. R., and Meneveau, C., "The Fractal Facets of Turbulence," *Journal of Fluid Mechanics*, Vol. 173, Dec. 1986, pp. 357–386.

[19]Tennekes, H., and Wyngaad, J. C., "The Intermittent Small Scale Structure of Turbulence: Data Processing Hazards," *Journal of Fluid Mechanics*, Vol. 55, Pt. 1, Sept. 1972, pp. 93–103.

[20]Frenkiel, F. N., and Klebanoff, P. S., "Statistical Properties of Velocity Derivatives in a Turbulent Field," *Journal of Fluid Mechanics*, Vol. 48, Pt. 1, July 1971, pp. 183–205.

[21]Champagne, F. H., "The Fine Scale Structure of the Turbulent Velocity Field," *Journal of Fluid Mechanics*, Vol. 86, Pt. 1, May 1978, pp. 67–108.

[22]Antonia, R. A., Satyaprakash, B. R., and Hussain, A. K. M. F., "Fine Scale Velocity Statistics in Turbulence Plane and Circular Jets," *Journal of Fluid Mechanics*, Vol. 119, June 1982, pp. 55–89.

[23]Schedvin, J., Stegen, R. G., and Gibson, C. G., "Universal Similarity at High Grid Reynolds Numbers," *Journal of Fluid Mechanics*, Vol. 65, Pt. 3, Sept. 1974, pp. 561–579.

[24]Tennekes, H., and Lumley, J. L., *A First Course in Turbulence*, MIT Press, Cambridge, MA, 1972.

[25]Sreenivasan, K. R., Chambers, A. J., and Antonia, R. A., *Boundary Layer Met.*, Vol. 14, 1978, p. 341.

[26]ANSI/ASME PTC 19.1, "Measurement Uncertainty," 1984.

[27]Catalano, G. D., Chang, K. S., and Mathis, J. A., "Investigation of Turbulent Jet Impingement in a Confined Crossflow," *AIAA Journal*, Vol. 27, No. 11, 1989, pp. 1530–1535.

[28]Wyngaard, J. C., and Tennekes, H., "Measurements of Small Scale Structure of Turbulence at Moderate Reynolds Numbers," *Physics of Fluids*, Vol. 13, No. 8, 1970, pp. 1962–1969.